Insights into the complex formation of a trimeric autotransporter adhesin with a peptidoglycan-binding periplasmic protein

Running title: Complex formation of a TAA with a periplasmic protein

Shogo Yoshimoto[1], Jun Sasahara[1], Atsuo Suzuki[1], Junichi Kanie[1], Kotaro Koiwai[1], Andrei N. Lupas[2], Katsutoshi Hori[1,*]

[1] Department of Biomolecular Engineering, Graduate School of Engineering, Nagoya University, Nagoya 464-8603, Aichi, Japan

[2] Department of Protein Evolution, Max Planck Institute for Biology, 72076 Tübingen, Baden-Württemberg, Germany

* Correspondence: Katsutoshi Hori
Department of Biomolecular Engineering, Graduate School of Engineering, Nagoya University, Furo-cho, Chikusa-ku, Nagoya, Aichi 464-8603, Japan.
Tel: +81-52-789-3339
Email: khori@chembio.nagoya-u.ac.jp

Abstract word count: 229 words

Text word count: 4847 words (excluding the references, table footnotes, and figure legends)

Abstract

Trimeric autotransporter adhesins (TAAs) are outer membrane (OM) proteins that are widely distributed in gram-negative bacteria and are involved primarily in adhesion to biotic and abiotic surfaces, cell agglutination, and biofilm formation. TAAs consist of a passenger domain, which is secreted onto the cell surface, and a transmembrane domain, which forms a pore in the OM to secrete and anchor the passenger domain. Because the interactions between TAAs and chaperones or dedicated auxiliary proteins during secretion are short-lived, TAAs are thought to reside on the OM without forming complexes with other proteins after secretion. In this study, we aimed to clarify the interactions between an *Acinetobacter* TAA, AtaA, and a peptidoglycan (PG)-binding periplasmic protein, TpgA. Pull-down assays using recombinant proteins identified the interacting domains. X-ray crystallography at 2.6 Å resolution revealed an A3B3 heterohexameric complex structure composed of the N-terminal domain of TpgA and the transmembrane domain of AtaA. TpgA-N consists of two short α helices and three antiparallel β strands, yielding an ααβββ topology similar to BamE. However, the regions corresponding to BamE interfaces with BamA and BamD differ in TpgA-N. All-atom molecular dynamics simulations and mutational assays revealed that both electrostatic and hydrophobic interactions contribute to stable complex formation. Bioinformatic analyses indicate that the TAA-TpgA complex occurs in a wide range of species. These findings will contribute to a better understanding of TAAs and the cell envelope.

Importance

Gram-negative bacteria have specialized secretion systems (SSs) that translocate molecules from the cytoplasm to the extracellular space. Type V SSs have a simpler structure consisting of a functional passenger domain and a transmembrane domain involved in the secretion and anchoring of the passenger domain. Here, we provide the first direct evidence that a trimeric autotransporter adhesin (TAA) exported by a type Vc system forms a stable complex with a peptidoglycan-binding periplasmic protein. The 2.6 Å structure of the A3B3 heterohexamer, together with simulation and mutational data, reveals complementary electrostatic and hydrophobic contacts that stabilize flexible loops on the periplasmic face of the TAA transmembrane barrel. Conservation of the *taa-tpgA* gene cassette and of key interface residues across diverse genera suggests that this coupling is a common strategy for tuning TAA stability and indicates that the envelope architecture of many TAAs,

55 including those related to pathogenicity, is more elaborate than previously appreciated.

Main Text

Introduction

Cells of gram-negative bacteria are enveloped by the inner membrane, peptidoglycan (PG), and outer membrane (OM) (1). To translocate molecules from the cytoplasm to the extracellular space across these barriers, gram-negative bacteria have specialized secretion systems (SSs) known as type I to VI and VIII to XI (2-5). Molecules secreted through these SSs are responsible for various functions, including cell adhesion, immune evasion, toxin activity, stress response, motility, the transfer of genetic information, and substrate degradation. Therefore, understanding the structure and function of these SSs is important not only in microbiology but also for medical and bioengineering applications.

Type V SSs, known as autotransporters (6), have simpler architectures than that of the other types of SSs. These proteins can be further divided into subclasses, type Va to Ve SSs, which share a structure consisting of a passenger domain secreted into the extracellular space and a transmembrane domain involved in the secretion of the passenger domain through the OM and the anchoring of the passenger domain to the cell surface (Fig. S1)(7). In the type Vb SS only, the passenger and transmembrane domains are produced as separate molecules, and the other type V SSs are translated as a single molecule that contains both domains in the same polypeptide chain. In the type Va SS, which secretes monomeric autotransporters, the polypeptides synthesized in the cytoplasm pass through the inner membrane via the Sec system, and periplasmic chaperones, such as SurA, Skp, DegP, DnaK, and FkpA, assist this periplasmic transit (8-11). With the assistance of the β-barrel assembly machinery (BAM) complex, the transmembrane domain inserts into the OM as a 12-stranded β-barrel, and the passenger domain of the same molecule is transported to the extracellular milieu through a hybrid pore composed of the BAM complex and the transmembrane domain with no need for external energy sources (7, 12-14). The overall secretion process of the type Vc SS, another subtype of type V SSs that secretes trimeric autotransporter adhesins (TAAs) (15), is thought to be similar to that of the type Va SS, except that a trimeric intermediate is formed before membrane insertion (16). The passenger domain of TAAs usually remains on the cell surface after secretion due to anchoring by the transmembrane domain. In addition to the general periplasmic chaperones and BAM complex, in the type Vc SS, genes that form an operon with *taa* in the genome have also been reported to participate in the biogenesis of TAAs: the *Burkholderia* heptosyltransferase BimC participates in the localization of BimA to the cell pole (17), and

89 the *Salmonella* inner membrane lipoprotein SadB participates in the outer membrane
90 insertion of SadA (18, 19). The interaction between TAAs and chaperones or dedicated
91 auxiliary proteins is transient (18), and TAAs are thought to reside on the outer membrane
92 through its transmembrane domain without forming complexes with other proteins after
93 secretion.
94 The gram-negative bacterium *Acinetobacter* sp. Tol 5 shows extremely high
95 adhesiveness to various material surfaces, including hydrophobic plastics, hydrophilic
96 glass, and metals, through its TAA, AtaA (20). The polypeptide chains of AtaA, consisting
97 of 3,630 amino acids, form a very large homotrimeric fibrous structure that is more than 1
98 MDa in molecular weight and 260 nm in length (21). We previously reported that the *tpgA*
99 gene, which forms a single operon with *ataA*, is involved in the biogenesis of AtaA (22).
100 TpgA is characterized as a periplasmic protein composed of the SmpA/OmlA-like N-
101 terminal domain and the OmpA_C-like C-terminal domain containing a PG-binding motif.
102 The interaction between TpgA and AtaA was shown by a pulldown assay without
103 crosslinking (22), suggesting that TpgA forms a stable complex with AtaA rather than a
104 transient interaction.
105 In this study, we aimed to clarify the interaction between TpgA and AtaA. This study
106 provides structural insights into PG-binding periplasmic proteins that form stable
107 complexes with TAAs.
108
109 **Results**
110 **Identification of the interacting domains of AtaA and TpgA.**
111 To identify which region of AtaA binds to TpgA, we performed a pull-down assay using
112 recombinant AtaA fragments containing several AtaA domains, as shown in Fig. 1A.
113 $AtaA_{723\text{-}806}$, $AtaA_{1221\text{-}1416}$, $AtaA_{2215\text{-}2395}$, and $AtaA_{2777\text{-}2903}$ were designed to connect to both
114 the N- and the C-terminal trimeric GCN4 adaptors, GCN4pII, which have been used to
115 stabilize coiled-coil domains of TAA recombinant proteins (23). $AtaA_{3524\text{-}3630}$ was designed
116 to be fused to the N-terminal OmpA signal sequence for secretion and presentation on the
117 outer membrane in *Escherichia coli* because it contains the transmembrane domain. We
118 also used previously constructed expression plasmids for $AtaA_{59\text{-}325}$, $AtaA_{2905\text{-}3168}$, and
119 $AtaA_{3170\text{-}3561}$ (24, 25). All of these recombinant proteins were connected to a C-terminal
120 His-tag except for $AtaA_{3524\text{-}3630}$ which was connected to the N-terminal signal sequence
121 followed by His-tag. Considering the repetitive sequences, these recombinant proteins

122 cover almost the entire region of AtaA. The cell lysate of Tol 5 Δ*ataA*, which contained
123 native TpgA, was mixed with recombinant AtaA fragment-bound nickel-nitrilotriacetic acid
124 (Ni-NTA) beads, and the pulled-down proteins were subjected to SDS–PAGE and detected
125 by CBB staining and western blotting using an anti-TpgA antibody. All of the recombinant
126 proteins of AtaA fragments immobilized on the beads were detected by CBB staining, but
127 TpgA was detected only in the sample incubated with the beads to which $AtaA_{3524-3630}$ had
128 been bound (Fig. 1B). These results suggest that TpgA specifically binds to $AtaA_{3524-3630}$,
129 the C-terminal region containing the transmembrane domain.
130 Next, to determine which domain of TpgA binds to AtaA, we performed a pull-down
131 assay using recombinant TpgA or its domains. $TpgA_{24-264}$ have been previously designed
132 with its signal sequence removed. $TpgA_{24-138}$ and $TpgA_{139-264}$ consist of the N- and C-
133 terminal domains of TpgA, respectively. All of these recombinant proteins were connected
134 to a His-tag. The cell lysate of Tol 5 Δ*tpgA*, which contained native AtaA, was mixed with
135 recombinant TpgA (or TpgA domain)-bound Ni-NTA beads, and the pulled-down proteins
136 were subjected to SDS–PAGE and detected by CBB staining and western blotting using an
137 anti-AtaA antiserum. AtaA was pulled down with $TpgA_{24-264}$ and $TpgA_{24-138}$ but not with
138 $TpgA_{139-264}$ (Fig. 1C). These results suggest that the transmembrane domain of AtaA (AtaA-
139 TM) forms a complex with the N-terminal domain of TpgA (TpgA-N).
140
141 **Crystal structure of the transmembrane domain of AtaA in complex with the N-**
142 **terminal domain of TpgA.**
143 To determine the structure of AtaA-TM in complex with TpgA-N, we attempted to purify
144 the protein complex of AtaA-TM and TpgA-N. The cell lysate of *E. coli* expressing His-
145 tagged $TpgA_{24-138}$ was added to a Ni-NTA column, which was washed to remove the
146 unbound proteins. The OmpA signal sequence-fused $AtaA_{3524-3630}$ without a His-tag was
147 expressed in *E. coli,* and the membrane fraction solubilized by a detergent was added to the
148 $TpgA_{24-138}$-bound Ni-NTA column for the formation of the protein complex. After the
149 unbound proteins were washed out, the protein complex was eluted with imidazole solution
150 and further purified by size-exclusion chromatography. As shown in Fig. 2A and 2B, highly
151 pure AtaA-TM in complex with TpgA-N was obtained at the elution peak corresponding to
152 82 kDa. This molecular weight was very close to that of three molecules of 11.1 kDa AtaA-
153 TM and three molecules of 14.9 kDa TpgA-N (78 kDa), suggesting that AtaA-TM and
154 TpgA-N form a stable A3B3 heterohexamer complex.

155 After crystallization screens using the purified protein complex, we determined the
156 structure of AtaA-TM in complex with TpgA-N at 2.6 Å resolution by X-ray
157 crystallography (Fig. 2C, PDB ID: 9VNJ). This is the first report showing a quaternary
158 structure of the transmembrane domain of TAA in complex with another protein. Three
159 molecules of TpgA-N bind to the periplasmic side of the homotrimeric transmembrane β-
160 barrel of AtaA-TM, forming the A3B3 heterohexamer, as estimated by size exclusion
161 chromatography. The monomer of AtaA-TM contains an N-terminal helix followed by a
162 four-stranded β-sheet, and a 12-stranded β-barrel is formed through homotrimerization. As
163 shown in Fig. 2D, the structure of AtaA-TM is very similar to the previously determined
164 structures of transmembrane domains of other TAAs, such as those of *Haemophilus*
165 *influenzae* Hia and *Yersinia enterocolitica* YadA (26, 27). The structure of TpgA-N consists
166 of two small α-helices and three antiparallel β-strands with an ααβββ topology (Fig. 2E).
167 The two α-helices pack against the β-sheet, forming an α/β 2-layer sandwich architecture.
168 The most similar known protein is that of *E. coli* BamE (28). While they share 27% amino
169 acid sequence identity, the structures differ with a root-mean-square deviation (RMSD) of
170 3.7 Å, particularly in the N-terminal region and in the β1- and β2-strands, which are
171 involved in the binding of BamE to BamA and BamD (Figs. 2F and S2) (29).
172
173 **Interaction between the transmembrane domain of AtaA and the N-terminal domain**
174 **of TpgA.**
175 To investigate how AtaA and its TpgA complex behave in the outer membrane, we
176 conducted all-atom molecular dynamics (MD) simulations. The crystal structures of AtaA-
177 TM and the complex of AtaA-TM and TpgA-N were embedded in an asymmetric lipid
178 membrane: the upper leaflet consisted of lipopolysaccharides (LPS) derived from
179 *Acinetobacter baumannii* and the lower leaflet composed of a mixture of 1-palmitoyl-2-
180 oleoyl-*sn*-glycero-3-phosphoethanolamine (POPE) and 1-palmitoyl-2-oleoyl-*sn*-glycero-3-
181 phosphatidylglycerol (POPG) in a 4:1 ratio, which mimicked the reported *Acinetobacter*
182 lipid composition (30) (Fig. 3A). The structure of AtaA-TM reached equilibrium during the
183 500 ns simulation, and no significant difference was observed in its RMSD in the presence
184 or absence of TpgA (Fig. S3). Calculation of per-residue RMSF of AtaA-TM showed that
185 residues 3573 to 3576, which form the periplasm-exposed α-helix to β1 loop, and residues
186 3601 to 3604, which form the β2 to β3 loop, exhibited decreased RMSF upon TpgA
187 binding (Fig. 3B). In YadA from *Y. enterocolitica*, the β2 to β3 loop has also been reported

188 to be flexible (31). These data indicate that complex formation with TpgA stabilizes these
189 loops of AtaA-TM. The loops are positioned adjacent to the hydrophobic tip of TpgA
190 containing L80 and F81 and are in proximity to two electrostatic pairs, K64–D3601 and
191 D65–K3576, which likely provide the stabilizing contacts (Fig. 3C). To examine the extent
192 to which these interactions contribute to complex formation, we performed a pull-down
193 assay using point-mutated TpgA-N proteins. The cell lysate of Tol 5 Δ*tpgA*, which
194 contained native AtaA, was mixed with mutated TpgA-bound Ni-NTA beads, and the
195 pulled-down proteins were subjected to SDS–PAGE and detected by CBB staining. As
196 shown in Fig. 3D, the D65A and L80A mutations did not affect complex formation between
197 AtaA-TM and TpgA-N, but the K64A and F81A mutations reduced complex formation.
198 The K64A/D65A and L80A/F81A double mutations reduced the interaction. These results
199 indicate that both electrostatic and hydrophobic interactions caused by these residues are
200 important for complex formation.
201
202 **Bioinformatic analysis of the AtaA-TpgA interaction.**
203 To clarify whether the TAA-TpgA complex exists in a wide range of species, we
204 performed bioinformatic analysis. The amino acid sequences with similarity to that of
205 TpgA-N were collected using BLAST and clustered based on sequence similarity using
206 CLANS (32). As shown in Fig. 4A, eight clusters were observed. TpgA-like sequences
207 formed cluster I, which was different from clusters II and III containing a typical
208 SmpA/OmlA family protein, BamE. Cluster I included sequences from a wide range of
209 Pseudomonadota (Proteobacteria), such as *Altererythrobacter*, *Burkholderia*, *Neisseria*,
210 *Acinetobacter*, *Stenotrophomonas*, *Escherichia*, and *Campylobacter*, as shown in Table S1.
211 The domain composition of the sequences differed from cluster to cluster (Fig. 4A). In
212 cluster I, approximately 80% of the sequences have an OmpA_C domain in the C-terminus,
213 similar to that in TpgA, and most of the sequences in clusters II, III, IV, and V have no
214 extra domain. Those in clusters VI and VII have a domain of unknown function (DUF) in
215 the N-terminus, and those in cluster VIII have a DUF in the C-terminus. Thus, the domain
216 structure of the sequences in cluster I, including TpgA, which consists of an N-terminal
217 SmpA/OmlA domain and a C-terminal OmpA_C domain, is distinct and unique among
218 proteins that contain the SmpA/OmlA domain.
219 In addition, 91% of the sequences in cluster I were downstream of the *taa* gene in the
220 genome, although those in other clusters were rarely near the *taa* gene. This result is

221 consistent with a previous finding that the occurrence of *ata*, a TAA of *Acinetobacter*
222 *baumannii*, in the genome was tightly linked to that of *tpgA* (33). In the *taa-tpgA* gene
223 cassette found in cluster I, L80 and F81 of TpgA were conserved as hydrophobic and
224 aromatic residue pairs, respectively (Fig. 4B). Furthermore, K64 of TpgA and D3601 of
225 AtaA, which interact with each other, are also conserved (Fig. 4B, C). In contrast, D3601 is
226 not conserved in TAAs that do not form the *taa-tpgA* gene cassette, such as YadA (27),
227 BadA (34), or UpaG (35), except for Hia (26), suggesting that D3601 of TAAs for which
228 *tpgA* exists downstream in the genome, is conserved because of its interaction with TpgA.
229 These new findings suggest that the TAA-TpgA protein complex is formed in a wide range
230 of species.
231
232
233 **Discussion**
234 TAAs interact with various auxiliary proteins during secretion but are thought to consist of
235 simple components after secretion. In this study, we revealed that TpgA forms a
236 heterohexamer with AtaA (Fig. 2). This is the first report directly showing that the
237 transmembrane domain of TAA forms a stable complex with periplasmic proteins.
238 While each SS of type Va to Ve secretes a variety of passenger domains into the
239 extracellular space or onto the cell surface, they share a common feature in that the
240 transmembrane domain is anchored only to the OM, except for some type Ve SSs, which
241 have a PG-binding LysM domain on the periplasmic side of their own polypeptide chain
242 (Fig. S1) (36). AtaA does not have a PG-binding domain, but TpgA has a PG-binding
243 domain containing the OmpA_C-like sequence at the C-terminus, and it was shown that
244 TpgA actually isolated with PG (22). Considering that the N-terminal domain of TpgA
245 binds to the C-terminal transmembrane domain of AtaA (Figs. 1, 2), these proteins likely
246 form the AtaA-TpgA-PG complex (Fig. 5). In mammalian cells, the cell adhesion protein
247 cadherin also forms a complex with actin filaments via catenins (37, 38). This implies that
248 anchoring cell adhesion proteins to the structures involved in cell shape and strength, such
249 as the cytoskeleton or peptidoglycan, would be universally important for mechanical
250 stabilization.
251 The overall structure of TpgA-N was similar to that of BamE, but the structures of the
252 regions of BamE that bind to BamA and BamD (29) and the corresponding region of TpgA-
253 N were different (Figs. 2F and S2). Furthermore, clustering analysis revealed that the *tpgA*-

like genes formed a distinct cluster from other SmpA/OmlA family genes, such as *bamE* (Fig. 4A), and the TpgA residues interacting with AtaA were not conserved in BamE (Fig. S2). These results indicate that TpgA does not function as a subunit of the BAM complex. When TpgA was used as bait to isolate the protein complex of AtaA-TM and TpgA-N, the other β-barrel proteins were not co-isolated from *E. coli* lysate with TpgA-N (Fig. 2B). This indicates that TpgA does not bind nonspecifically to β-barrel proteins but rather specifically to AtaA, via the hydrophobic and electrostatic interactions (Fig. 3).

The *tpgA*-like genes were found widely in the strains belonging to Pseudomonadota (Proteobacteria), and most of them were located downstream of the *taa* genes in the genome (Fig. 4 and Table S1). These findings suggest that the TAA-TpgA protein complex is formed in a wide range of species. Notably, the clinically relevant pathogen *A. baumannii* also possesses a TAA-TpgA cassette as previously reported (33, 39), suggesting that TpgA may promote TAA-dependent virulence in pathogenic bacteria; dedicated experimental studies are still needed to confirm this possibility.

In conclusion, we revealed the structure of a PG-binding periplasmic protein that forms a stable complex with the transmembrane domain of a TAA. Our findings will contribute to a better understanding of the type Vc SS and the control of TAA-mediated adhesion, which is important for medical and engineering applications.

Materials and Methods

Bacterial strains and growth conditions.

The bacterial strains and plasmids used in this study are listed in Table S2. *Acinetobacter* sp. Tol 5 and its derivative strains were grown in basal salt medium supplemented with toluene or in Luria–Bertani (LB) medium at 28°C, as described previously (20). *E. coli* DH5α, BL21(DE3), and their derivative strains were grown in LB medium supplemented with 100 μg/ml ampicillin for cells harboring pASK-IBA plasmids or with 50 μg/ml kanamycin for cells harboring pET plasmids at 37°C.

Construction of plasmids.

The primers used in this study are listed in Table S3. To construct plasmids expressing a recombinant AtaA fragment fused to a GCN4pII-tag at both the N- and C-termini and a His-tag at the C-terminus, DNA fragments encoding $AtaA_{723\text{-}806}$, $AtaA_{1221\text{-}1416}$, $AtaA_{2215\text{-}2395}$,

287 or $AtaA_{2777-2903}$ were amplified via PCR and inserted into the BsaI site of the *E. coli*
288 expression vector pIBA-GCN4tri-His (23). To construct a plasmid expressing $AtaA_{3524-3630}$
289 fused to the His-tag at the N-terminus at the OM, the DNA fragment encoding this gene
290 was amplified via PCR and inserted between the NheI and HindIII sites of the *E. coli*
291 expression vector pASK-IBA12 (IBA Lifesciences, Göttingen, Germany), generating
292 pIBA-His-$AtaA_{3524-3630}$. To remove the His-tag sequence from pIBA-His-$AtaA_{3524-3630}$, a
293 DNA fragment was amplified via PCR using pIBA-His-$AtaA_{3524-3630}$ as a template with two
294 primers (TM-dHis-f/r) and then self-ligated, generating pIBA-$AtaA_{3524-3630}$. To construct
295 plasmids expressing $TpgA_{24-138}$, $TpgA_{139-264}$ or the point mutated TpgAs fused to a His-tag
296 at the C-terminus, a DNA fragment was amplified via PCR using pET28d::$TpgA_{24-264}$ (24)
297 as a template with corresponding primer sets and then self-ligated, generating
298 pET28d::$TpgA_{24-138}$, pET28d::$TpgA_{139-264}$, and plasmids for the point-mutated TpgAs.
299
300 **Protein purification.**
301 To purify the complex of TpgA-N and AtaA-TM, an overnight culture of BL21 (DE3;
302 pET28d::$TpgA_{24-264}$) was diluted 1:100 in LB medium and incubated for 3 h at 37°C. After
303 incubation, isopropyl β-D-thiogalactopyranoside (IPTG) (final concentration: 0.1 mM) was
304 added to the medium, and the culture was further incubated at 18°C for 18 h. The cells were
305 harvested by centrifugation at 5,000×*g* at 4°C for 15 min, resuspended in lysis buffer (25
306 mM Tris-HCl, 150 mM NaCl, 20 mM imidazole, pH 9.0) supplemented with 0.1 mg/ml
307 lysozyme, and lysed using a high-pressure homogenizer (LAB 2000; SMT Co., Tokyo,
308 Japan) at 1,000 bar for 10 min. After centrifugation at 10,000×*g* at 4°C for 15 min, the
309 supernatant was loaded onto a Ni-NTA Superflow column (Qiagen, Venlo, Netherlands),
310 and the unbound proteins were washed off with lysis buffer. Subsequently, an overnight
311 culture of BL21 (DE3; pIBA-$AtaA_{3524-3630}$) was diluted 1:100 in LB medium and incubated
312 for 3 h at 37°C. After incubation, anhydrotetracycline (AHTC) (final concentration: 0.2
313 μg/ml) was added to the medium, and the mixture was further incubated at 28°C for 12 h.
314 The cells were harvested by centrifugation at 5,000×*g* at 4°C for 15 min, resuspended in
315 lysis buffer supplemented with 0.1 mg/ml lysozyme, and lysed using a high-pressure
316 homogenizer at 1,000 bar for 10 min. After centrifugation at 5,000×*g* at 4°C for 15 min, the
317 supernatant was ultracentrifuged at 100,000×*g* at 4°C for 2 h, and the precipitate was
318 solubilized with 5% Elugent (Merck, Darmstadt, Germany) and suspended in Elugent
319 buffer A (25 mM Tris-HCl, 150 mM NaCl, 20 mM imidazole, 0.5% Elugent, pH 9.0). The

320 suspension was loaded onto a TpgA-N-bound Ni-NTA column, and unbound proteins were
321 washed off with Elugent buffer A. The bound proteins were eluted with Elugent buffer A
322 supplemented with 300 mM imidazole and loaded onto a HiLoad 26/60 Superdex 75 pg
323 column (Cytiva, Marlborough, MA) equilibrated with 25 mM Tris-HCl (pH 7.5) buffer
324 containing 10 mM NaCl and 0.5% Elugent. Peak fractions containing the protein complex
325 were dialyzed using a 12-14 kD MWCO dialysis membrane (Spectrum Laboratories,
326 Rancho Dominguez, CA) against Elugent buffer B (25 mM Tris-HCl, 10 mM NaCl, 0.5%
327 Elugent, pH 9.0) and loaded onto a HiTrap Q HP column (Cytiva) equilibrated with Elugent
328 buffer B. The column was washed three times with 0.6% tetraethylene glycol monooctyl
329 ether (C8E4) containing 25 mM Tris-HCl (pH 9.0) and 10 mM NaCl and two times with
330 0.6% C8E4 containing 25 mM Tris-HCl (pH 9.0) and 100 mM NaCl. The bound proteins
331 were eluted with 0.6% C8E4 containing 25 mM Tris-HCl (pH 9.0) and 500 mM NaCl,
332 dialyzed against crystallization buffer (25 mM Tris-HCl, 10 mM NaCl, 0.6% C8E4, pH
333 8.0), and concentrated by ultrafiltration using a 10 kDa cutoff filter device (Amicon Ultra;
334 Merck).
335 $TpgA_{24-264}$, $TpgA_{24-138}$ (TpgA-N), and $TpgA_{139-264}$ (TpgA-C) were purified as described
336 previously (22). In brief, cells expressing each protein were harvested and lysed using a
337 high-pressure homogenizer. After centrifugation, the protein was purified from the
338 supernatant by Ni-affinity chromatography, ion-exchange chromatography, and size-
339 exclusion chromatography.
340
341 **Pull-down assay.**
342 For the pull-down assay using recombinant AtaA fragments and cell lysate containing
343 TpgA, an overnight culture of BL21 (DE3) cells harboring plasmids expressing
344 recombinant AtaA fragments was diluted 1:100 in LB medium and incubated for 3 h at
345 37°C. After incubation, AHTC (final concentration: 0.2 μg/ml) was added to the medium
346 and further incubated at 28°C for 12 h. The cells were harvested by centrifugation at
347 5,000×*g* at 4°C for 15 min, resuspended in pull-down buffer A (25 mM Tris-HCl, 10 mM
348 NaCl, 0.1% Tween 20, 20 mM imidazole, pH 7.5), and lysed by sonication. After
349 centrifugation at 10,000×*g* at 4°C for 10 min, 500 μl of the supernatant (2 mg/ml) was
350 mixed with 10 μl of Ni-NTA Superflow. After 2 h of incubation on a rotary mixer (NRC-
351 20D; Nissinrika, Tokyo, Japan) at 5 rpm and 4°C, the beads were pelleted by centrifugation
352 at 1,000×*g* for 1 min at 4°C and rinsed three times with pull-down buffer A. The beads were

353 mixed with 500 μl of 5 mg/ml cell lysate from Tol 5 Δ*ataA* and incubated for 2 h on a
354 rotary mixer at 4°C. The beads were pelleted by centrifugation at 1,000×*g* for 1 min at 4°C
355 and rinsed three times with pull-down buffer A. The bound proteins were eluted with 50 μl
356 of 300 mM imidazole (pH 7.5), mixed with 50 μl of 2×SDS–PAGE sample buffer, and
357 boiled at 98°C for 10 min. The protein samples were separated by SDS–PAGE and
358 subjected to CBB staining and western blotting analysis with an anti-TpgA antibody (22).
359 For the pull-down assay using recombinant TpgA fragments and cell lysate containing
360 AtaA, 50 μg of His-tagged $TpgA_{24-264}$, His-tagged $TpgA_{24-138}$, or His-tagged $TpgA_{139-264}$
361 suspended in 300 μl of pull-down buffer A was mixed with 10 μl of Ni-NTA Superflow.
362 After 1 h of incubation on a rotary mixer at 4°C, the beads were pelleted by centrifugation
363 at 1,000×*g* for 1 min at 4°C, rinsed three times with pull-down buffer A, and resuspended in
364 300 μl of pull-down buffer A. To prepare the cell lysate of Tol 5 Δ*tpgA*, 100 ml of the cell
365 suspension at an OD_{660} of 0.6 was harvested by centrifugation at 5,000×*g* for 10 min at 4°C
366 and resuspended in 2 ml of BugBuster (Merck), and 50 μg/ml lysozyme and 1 mM
367 phenylmethanesulfonyl fluoride (PMSF) were added. Unlysed cells and debris were
368 removed by centrifugation at 10,000×*g* for 10 min at 4°C. Finally, 200 μl of the cell lysate
369 was mixed with 300 μl of TpgA fragment-bound Ni-NTA beads suspended in pull-down
370 buffer A and incubated on a rotary mixer at 4°C for 2 h. The beads were pelleted by
371 centrifugation at 1,000×*g* for 1 min at 4°C and rinsed with pull-down buffer A for removal
372 of unbound proteins. The bound proteins were eluted with 50 μl of 300 mM imidazole (pH
373 7.5), mixed with 50 μl of 2×SDS–PAGE sample buffer, and boiled at 98°C for 10 min. The
374 protein samples were separated via SDS–PAGE and subjected to CBB staining and western
375 blotting analysis with anti- $AtaA_{699-1014}$ antiserum.
376 For the pull-down assay using TpgA mutants and cell lysates containing AtaA-TM, 10 μg
377 of His-tagged TpgA variants suspended in 1 ml of pull-down buffer B (25 mM Tris-HCl,
378 150 mM NaCl, 20 mM imidazole, 0.6% Elugent, pH 7.0) was mixed with 10 μl of Ni-NTA
379 Superflow. After a 1-h incubation on a rotary mixer at 4°C, the beads were pelleted by
380 centrifugation at 1,000×*g* for 1 min at 4°C and rinsed three times with pull-down buffer B.
381 The beads were mixed with 1 ml of 1 mg/ml cell lysate containing AtaA-TM suspended in
382 pull-down buffer B and incubated for 1 h on a rotary mixer at 4°C. The beads were pelleted
383 by centrifugation at 1,000×*g* for 1 min at 4°C and rinsed three times with pull-down buffer
384 B. The bound proteins were then eluted with 25 μl of 500 mM imidazole (pH 7.5), mixed
385 with 25 μl of 2×SDS–PAGE sample buffer, and boiled at 98°C for 10 min. The protein

386 samples were separated by SDS–PAGE and subjected to CBB staining.
387
388 **Crystallization and X-ray crystallography.**
389 The crystallization conditions for the purified protein were first screened by using the
390 sitting-drop vapor-diffusion method at 20°C under 240 conditions using MemPlus
391 (Molecular Dimensions, Sheffield, UK), MemGold (Molecular Dimensions), and The
392 Protein Complex Suite (Qiagen). One microliter of 4.6 mg/ml protein sample suspended in
393 crystallization buffer (25 mM Tris-HCl, 10 mM NaCl, 0.6% C8E4, pH 8.0) and 1 μl of
394 reservoir solution were mixed and periodically observed for 2 weeks under a polarized
395 microscope (BH-2; Olympus). The final optimized crystallization conditions were as
396 follows: 0.2 M MES, 0.4 M calcium chloride, and 35% polyethylene glycol 400 at pH 5.0.
397 The crystal was loop-mounted and quenched in liquid nitrogen. The diffraction of the
398 crystals was measured under a cryo-condition at the synchrotron beamline NW-12A of the
399 Photon Factory (Tsukuba, Japan) by using a CCD detector (Quantum 270; ADSC, Poway,
400 CA). Diffraction images were processed and scaled by using HKL2000 (40). The CCP4
401 program suite was used for model building and refinement (41). The phases of all the
402 structures were determined by molecular replacement using MOLREP. The structure was
403 solved using the Hia transmembrane domain (PDB: 2GR7) as the search model. After the
404 molecular replacement, the structures were automatically built by ARP/wARP, manually
405 modeled with Coot, and refined by REFMAC5 and PHENIX (42). The crystallographic
406 parameters are summarized in Table S4. The final coordinates and structure factors that
407 support the findings of this study have been deposited in the PDB with the accession code
408 9VNJ.
409
410 **Bioinformatics.**
411 To obtain sequences with similarity to the N-terminal domain of TpgA, the NR70 database
412 was searched for the amino acid sequence of $TpgA_{24\text{-}138}$ using PSI-BLAST on the MPI
413 Bioinformatics Toolkit (43). We retrieved 1,461 sequences (E-value <0.001), and the
414 retrieved sequences were clustered using CLANS (32) at a P-value cutoff of 1e-10, an
415 attract value of 10 and a repulse value of 10. The multiple sequence alignment was
416 generated using ClustalO. The DNA sequence of *taa*, which is encoded upstream of the
417 *tpgA*-like gene, was collected from the NCBI nucleotide database. We searched for protein

structures similar to that of TpgA-N and calculated the root mean square deviation (RMSD) via the Dali server (44).

Molecular dynamics (MD) simulations

Using the crystal structure of the protein complex of AtaA-TM and TpgA-N (PDB ID: 9VNJ), two simulation systems were constructed with CHARMM-GUI (45): one consisting of the AtaA-TM and TpgA-N complex, and the other containing only AtaA-TM, with the TM region embedded in a lipid membrane. The lipid membrane was positioned at the center of the simulation box, which was then filled with water molecules. The overall system size was 8.1 nm × 8.1 nm × 16.5 nm. The membrane was asymmetric: the upper leaflet consisted of lipopolysaccharides (LPS) derived from *Acinetobacter baumannii*, with Ca^{2+} ions used to neutralize the negatively charged lipid A and core oligosaccharide regions, while the lower leaflet was composed of a mixture of 1-palmitoyl-2-oleoyl-*sn*-glycero-3-phosphoethanolamine (POPE) and 1-palmitoyl-2-oleoyl-*sn*-glycero-3-phosphatidylglycerol (POPG) in a 4:1 ratio. The LPS in the outer leaflet was modeled as a smooth structure, with the following glycan sequence: α-D-Glc (1→2) β-D-Glc (1→4) β-D-Glc (1→4) β-D-Glc (1→3) [β-D-GalN (1→4)] α-D-GlcNAc (1→4) [β-D-GlcN (1→7)] α-D-Kdo (2→5) [α-D-Kdo (2→4)] α-D-Kdo (2→lipid A). The CHARMM36m force field (46) in combination with the CHARMM-modified TIP3P water model (47) was used to describe all systems. The concentration of sodium chloride ions was set to 0.15 M. All MD simulations were performed using GROMACS 2020 (48). Simulations were conducted under NPT ensemble periodic boundary conditions, where the temperature was controlled at 301.15 K using the V-rescale method (49). The pressure was maintained at 1.0 bar using the Parrinello–Rahman method (50). Bonds involving hydrogen atoms were constrained using the LINCS method (51), and Coulomb interactions were calculated using the particle mesh Ewald (PME) method (52). The Lennard–Jones interactions and real-space PME calculations were set with a cutoff distance of 1.2 nm, and the grid size for the reciprocal-space calculations was set to ensure a grid spacing of 0.1 nm. The time step for all simulations was set to 2 fs. For each system, a 500 ns MD simulation was performed. The RMSD of the atoms corresponding to AtaA-TM was calculated, and the root mean square fluctuation (RMSF) was determined for each residue of AtaA-TM, followed by averaging the RMSF across the three chains.

Data Availability

Crystallographic coordinates and structure factors have been deposited in the PDB under accession code 9VNJ.

Acknowledgments

We thank Jens Bassler, Ryuta Hiroshige, Ayumi Hayashi, and Eriko Kawamoto for their technical assistance. We also thank Dirk Linke of the University of Oslo and Masahito Ishikawa of Nagahama Institute of Bio-Science and Technology for helpful discussion. This work was supported by the Japan Society for the Promotion of Science (JSPS) KAKENHI (Grant Numbers JP21H05227 and JP24H00043).

Author Contributions: K.H. and S.Y. designed the study and wrote the paper. S.Y., A.S., and K.K. prepared the recombinant proteins and conducted the structural analysis. S.Y. and A.L. conducted the bioinformatic analysis. J.S. conducted the molecular simulations. S.Y. and J.K. conducted the other biochemical experiments. All the authors reviewed the manuscript.

References

1. Sun JW, Rutherford ST, Silhavy TJ, Huang KC. 2022. Physical properties of the bacterial outer membrane. Nature Reviews Microbiology 20:236-248.
2. Costa TRD, Felisberto-Rodrigues C, Meir A, Prevost MS, Redzej A, Trokter M, Waksman G. 2015. Secretion systems in Gram-negative bacteria: structural and mechanistic insights. Nature Reviews Microbiology 13:343-359.
3. Palmer T, Finney AJ, Saha CK, Atkinson GC, Sargent F. 2021. A holin/peptidoglycan hydrolase-dependent protein secretion system. Molecular Microbiology 115:345-355.
4. Grossman AS, Mauer TJ, Forest KT, Goodrich-Blair H. 2021. A widespread bacterial secretion system with diverse substrates. Mbio 12.
5. Lauber F, Deme JC, Lea SM, Berks B. 2018. Type 9 secretion system structures reveal a new protein transport mechanism. Nature 564:77-82.
6. Klauser T, Pohlner J, Meyer TF. 1993. The secretion pathway of IgA protease-type proteins in gram-negative bacteria. Bioessays 15:799-805.

484 7. Leo JC, Grin I, Linke D. 2012. Type V secretion: mechanism(s) of autotransport
485 through the bacterial outer membrane. Philosophical Transactions of the Royal
486 Society B-Biological Sciences 367:1088-1101.
487 8. Purdy GE, Fisher CR, Payne SM. 2007. IcsA surface presentation in *Shigella*
488 *flexneri* requires the periplasmic chaperones DegP, Skp, and SurA. Journal of
489 Bacteriology 189:5566-5573.
490 9. Ruiz-Perez F, Henderson IR, Leyton DL, Rossiter AE, Zhang YH, Nataro JP. 2009.
491 Roles of periplasmic chaperone proteins in the biogenesis of serine protease
492 autotransporters of *Enterobacteriaceae*. Journal of Bacteriology 191:6571-6583.
493 10. Ruiz-Perez F, Henderson IR, Nataro- JP. 2010. Interaction of FkpA, a peptidyl-
494 prolyl cis/trans isomerase with EspP autotransporter protein. Gut Microbes 1:339-
495 344.
496 11. Janakiraman A, Fixen KR, Gray AN, Niki H, Goldberg MB. 2009. A genome-scale
497 proteomic screen identifies a role for DnaK in chaperoning of polar autotransporters
498 in *Shigell*. Journal of Bacteriology 191:6300-6311.
499 12. Voulhoux R, Bos MP, Geurtsen J, Mols M, Tommassen J. 2003. Role of a highly
500 conserved bacterial protein in outer membrane protein assembly. Science 299:262-
501 265.
502 13. Doyle MT, Jimah JR, Dowdy T, Ohlemacher SI, Larion M, Hinshaw JE, Bernstein
503 HD. 2022. Cryo-EM structures reveal multiple stages of bacterial outer membrane
504 protein folding. Cell 185:1143-1156.
505 14. Doyle MT, Bernstein HD. 2021. BamA forms a translocation channel for
506 polypeptide export across the bacterial outer membrane. Molecular Cell 81:2000-
507 2012.
508 15. Linke D, Riess T, Autenrieth IB, Lupas A, Kempf VAJ. 2006. Trimeric
509 autotransporter adhesins: variable structure, common function. Trends in
510 Microbiology 14:264-270.
511 16. Sikdar R, Peterson JH, Anderson DE, Bernstein HD. 2017. Folding of a bacterial
512 integral outer membrane protein is initiated in the periplasm. Nat Commun 8:1309.
513 17. Lu Q, Xu Y, Yao Q, Niu M, Shao F. 2015. A polar-localized iron-binding protein
514 determines the polar targeting of *Burkholderia* BimA autotransporter and actin tail
515 formation. Cell Microbiol 17:408-424.
516 18. Grin I, Hartmann MD, Sauer G, Hernandez Alvarez B, Schutz M, Wagner S,

517 Madlung J, Macek B, Felipe-Lopez A, Hensel M, Lupas A, Linke D. 2014. A
518 trimeric lipoprotein assists in trimeric autotransporter biogenesis in *Enterobacteria*.
519 J Biol Chem 289:7388-7398.
520 19. Hartmann MD, Grin I, Dunin-Horkawicz S, Deiss S, Linke D, Lupas AN, Alvarez
521 BH. 2012. Complete fiber structures of complex trimeric autotransporter adhesins
522 conserved in enterobacteria. Proceedings of the National Academy of Sciences of
523 the United States of America 109:20907-20912.
524 20. Ishikawa M, Nakatani H, Hori K. 2012. AtaA, a new member of the trimeric
525 autotransporter adhesins from *Acinetobacter* sp. Tol 5 mediating high adhesiveness
526 to various abiotic surfaces. PLoS One 7:e48830.
527 21. Yoshimoto S, Nakatani H, Iwasaki K, Hori K. 2016. An *Acinetobacter* trimeric
528 autotransporter adhesin reaped from cells exhibits its nonspecific stickiness via a
529 highly stable 3D structure. Sci Rep 6:28020.
530 22. Ishikawa M, Yoshimoto S, Hayashi A, Kanie J, Hori K. 2016. Discovery of a novel
531 periplasmic protein that forms a complex with a trimeric autotransporter adhesin
532 and peptidoglycan. Mol Microbiol 101:394-410.
533 23. Alvarez BH, Hartmann MD, Albrecht R, Lupas AN, Zeth K, Linke D. 2008. A new
534 expression system for protein crystallization using trimeric coiled-coil adaptors.
535 Protein Engineering Design & Selection 21:11-18.
536 24. Koiwai K, Hartmann MD, Linke D, Lupas AN, Hori K. 2016. Structural basis for
537 toughness and flexibility in the C-terminal passenger domain of an *Acinetobacter*
538 trimeric autotransporter adhesin. J Biol Chem 291:3705-24.
539 25. Aoki S, Yoshimoto S, Ishikawa M, Linke D, Lupas A, Hori K. 2020. Native display
540 of a huge homotrimeric protein fiber on the cell surface after precise domain
541 deletion. J Biosci Bioeng 129:412-417.
542 26. Meng G, Surana NK, St Geme JW, 3rd, Waksman G. 2006. Structure of the outer
543 membrane translocator domain of the *Haemophilus influenzae* Hia trimeric
544 autotransporter. The EMBO Journal 25:2297-304.
545 27. Shahid SA, Nagaraj M, Chauhan N, Franks TW, Bardiaux B, Habeck M, Orwick-
546 Rydmark M, Linke D, van Rossum BJ. 2015. Solid-state NMR study of the YadA
547 membrane-anchor domain in the bacterial outer membrane. Angewandte Chemie
548 International Edition 54:12602-6.
549 28. Gu Y, Li H, Dong H, Zeng Y, Zhang Z, Paterson NG, Stansfeld PJ, Wang Z, Zhang

550 Y, Wang W, Dong C. 2016. Structural basis of outer membrane protein insertion by
551 the BAM complex. Nature 531:64-69.
552 29. Kumar S, Konovalova A. 2023. BamE directly interacts with BamA and BamD
553 coordinating their functions. Molecular Microbiology 120:397-407.
554 30. Tao Y, Acket S, Beaumont E, Galez H, Duma L, Rossez Y. 2021. Colistin treatment
555 affects lipid composition of *Acinetobacter baumannii*. Antibiotics 10:528.
556 31. Yarava JR, Orwick-Rydmark M, Ryoo D, Hofstetter A, Gumbart JC, Habeck M, van
557 Rossum BJ, Linke D, Oschkinat H. 2025. Probing the dynamics of *Yersinia* adhesin
558 A (YadA) in outer membranes hints at requirements for β-barrel membrane
559 insertion. Journal of the American Chemical Society 147:8618-8628.
560 32. Frickey T, Lupas A. 2004. CLANS: a Java application for visualizing protein
561 families based on pairwise similarity. Bioinformatics 20:3702-3704.
562 33. Weidensdorfer M, Ishikawa M, Hori K, Linke D, Djahanschiri B, Iruegas R,
563 Ebersberger I, Riedel-Christ S, Enders G, Leukert L, Kraiczy P, Rothweiler F, Cinatl
564 J, Berger J, Hipp K, Kempf VAJ, Gottig S. 2019. The *Acinetobacter* trimeric
565 autotransporter adhesin Ata controls key virulence traits of *Acinetobacter*
566 *baumannii*. Virulence 10:68-81.
567 34. Kaiser PO, Linke D, Schwarz H, Leo JC, Kempf VAJ. 2012. Analysis of the BadA
568 stalk from *Bartonella henselae* reveals domain-specific and domain-overlapping
569 functions in the host cell infection process. Cellular Microbiology 14:198-209.
570 35. Valle J, Mabbett AN, Ulett GC, Toledo-Arana A, Wecker K, Totsika M, Schembri
571 MA, Ghigo JM, Beloin C. 2008. UpaG, a new member of the trimeric
572 autotransporter family of adhesins in uropathogenic *Escherichia coli*. Journal of
573 Bacteriology 190:4147-4161.
574 36. Leo JC, Oberhettinger P, Chaubey M, Schutz M, Kuhner D, Bertsche U, Schwarz H,
575 Gotz F, Autenrieth IB, Coles M, Linke D. 2015. The Intimin periplasmic domain
576 mediates dimerisation and binding to peptidoglycan. Molecular Microbiology
577 95:80-100.
578 37. Pokutta S, Weis WI. 2007. Structure and mechanism of cadherins and catenins in
579 cell-cell contacts. Annual Review of Cell and Developmental Biology 23:237-261.
580 38. Gooding JM, Yap KL, Ikura M. 2004. The cadherin-catenin complex as a focal
581 point of cell adhesion and signalling: new insights from three-dimensional
582 structures. BioEssays 26:497-511.

583 39. Li SK, Jiang GL, Wang SK, Wang M, Wu YL, Zhang JZ, Liu X, Zhong L, Zhou M,
584 Xie SC, Ren Y, He P, Lou YL, Li H, Du JM, Zhou ZM. 2025. Emergence and global
585 spread of a dominant multidrug-resistant clade within *Acinetobacter baumannii*.
586 Nature Communications 16:2787.
587 40. Otwinowski Z, Minor W. 1997. Processing of X-ray diffraction data collected in
588 oscillation mode. Methods in Enzymology 276:307-326.
589 41. Agirre J, Atanasova M, Bagdonas H, Ballard CB, Baslé A, Beilsten-Edmands J,
590 Borges RJ, Brown DG, Burgos-Mármol JJ, Berrisford JM, Bond PS, Caballero I,
591 Catapano L, Chojnowski G, Cook AG, Cowtan KD, Croll TI, Debreczeni JÉ,
592 Devenish NE, Dodson EJ, Drevon TR, Emsley P, Evans G, Evans PR, Fando M,
593 Foadi J, Fuentes-Montero L, Garman EF, Gerstel M, Gildea RJ, Hatti K, Hekkelman
594 ML, Heuser P, Hoh SW, Hough MA, Jenkins HT, Jiménez E, Joosten RP, Keegan
595 RM, Keep N, Krissinel EB, Kolenko P, Kovalevskiy O, Lamzin VS, Lawson DM,
596 Lebedev AA, Leslie AGW, Lohkamp B, Long F, Maly M, et al. 2023. The CCP4
597 suite: integrative software for macromolecular crystallography. Acta
598 Crystallographica Section D Structural Biology 79:449-461.
599 42. Liebschner D, Afonine PV, Baker ML, Bunkóczi G, Chen VB, Croll TI, Hintze B,
600 Hung LW, Jain S, McCoy AJ, Moriarty NW, Oeffner RD, Poon BK, Prisant MG,
601 Read RJ, Richardson JS, Richardson DC, Sammito MD, Sobolev OV, Stockwell
602 DH, Terwilliger TC, Urzhumtsev AG, Videau LL, Williams CJ, Adams PD. 2019.
603 Macromolecular structure determination using X-rays, neutrons and electrons:
604 recent developments in Phenix. Acta Crystallographica Section D 75:861-877.
605 43. Zimmermann L, Stephens A, Nam SZ, Rau D, Kubler J, Lozajic M, Gabler F,
606 Soding J, Lupas AN, Alva V. 2018. A completely reimplemented MPI
607 Bioinformatics Toolkit with a new HHpred server at its core. Journal of Molecular
608 Biology 430:2237-2243.
609 44. Holm L. 2020. DALI and the persistence of protein shape. Protein Science 29:128-
610 140.
611 45. Jo S, Kim T, Iyer VG, Im W. 2008. CHARMM-GUI: a web-based graphical user
612 interface for CHARMM. J Comput Chem 29:1859-65.
613 46. Huang J, Rauscher S, Nawrocki G, Ran T, Feig M, de Groot BL, Grubmuller H,
614 MacKerell AD, Jr. 2017. CHARMM36m: an improved force field for folded and
615 intrinsically disordered proteins. Nat Methods 14:71-73.

47. Jorgensen WL, Chandrasekhar J, Madura JD, Impey RW, Klein ML. 1983. Comparison of Simple Potential Functions for Simulating Liquid Water. Journal of Chemical Physics 79:926-935.
48. Mark James Abraham TM, Roland Schulz, Szilárd Páll, Jeremy C. Smith, Berk Hess, Erik Lindahl. 2015. GROMACS: High performance molecular simulations through multi-level parallelism from laptops to supercomputers. SoftwareX 1-2:19-25.
49. Bussi G, Donadio, D., & Parrinello, M. 2007. Canonical sampling through velocity rescaling. The Journal of chemical physics 126:014101.
50. Parrinello M, Rahman A. 1981. Polymorphic Transitions in Single-Crystals - a New Molecular-Dynamics Method. Journal of Applied Physics 52:7182-7190.
51. Hess B, Bekker H, Berendsen HJC, Fraaije JGEM. 1997. LINCS: A linear constraint solver for molecular simulations. Journal of Computational Chemistry 18:1463-1472.
52. Darden T, York D, Pedersen L. 1993. Particle Mesh Ewald - an N.Log(N) Method for Ewald Sums in Large Systems. Journal of Chemical Physics 98:10089-10092.

634 **Figure legends**

635

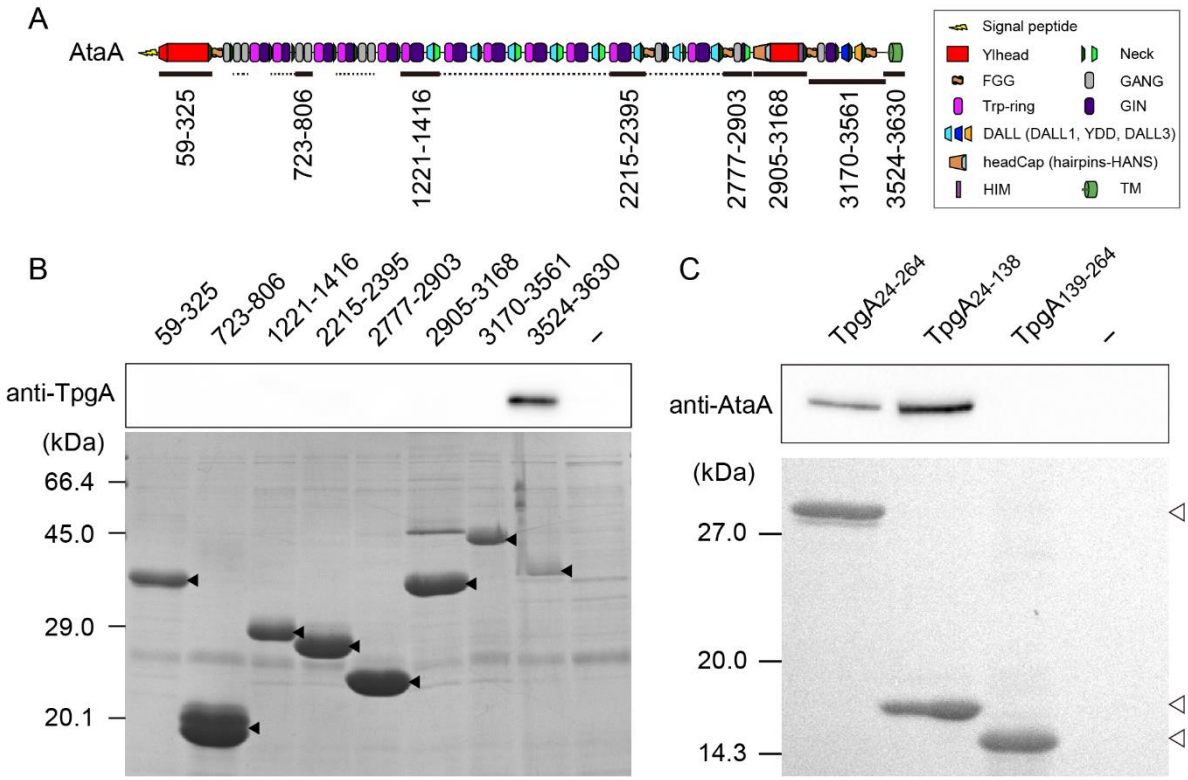

636

637 **Figure 1. Identification of the interacting domains of AtaA and TpgA.** (A) Schematic
638 structure of AtaA. The black lines show the region where the recombinant protein was
639 constructed, and the dotted lines show the region with high sequence similarity (>50%) to
640 the recombinant proteins. (B) Pull-down assay using recombinant AtaA fragments and
641 TpgA-containing cell lysate. The cell lysate of Tol 5 Δ*ataA* was mixed with recombinant
642 AtaA fragment-bound Ni-NTA beads or untreated beads (-). The pulled-down proteins were
643 subjected to SDS–PAGE and analyzed by western blotting to detect TpgA and CBB
644 staining to detect AtaA fragments. The solid triangles indicate recombinant AtaA
645 fragments. The upper numbers indicate the amino acid numbers of each recombinant AtaA
646 fragment immobilized onto Ni-NTA beads. (C) Pull-down assay using recombinant TpgA
647 fragments and AtaA-containing cell lysate. The cell lysate of Tol 5 Δ*tpgA* was mixed with
648 recombinant TpgA fragment-bound Ni-NTA beads or untreated beads (-). The pulled-down
649 proteins were subjected to SDS–PAGE and analyzed by western blotting to detect AtaA and
650 CBB staining to detect TpgA fragments. The open triangles indicate recombinant TpgA
651 fragments.

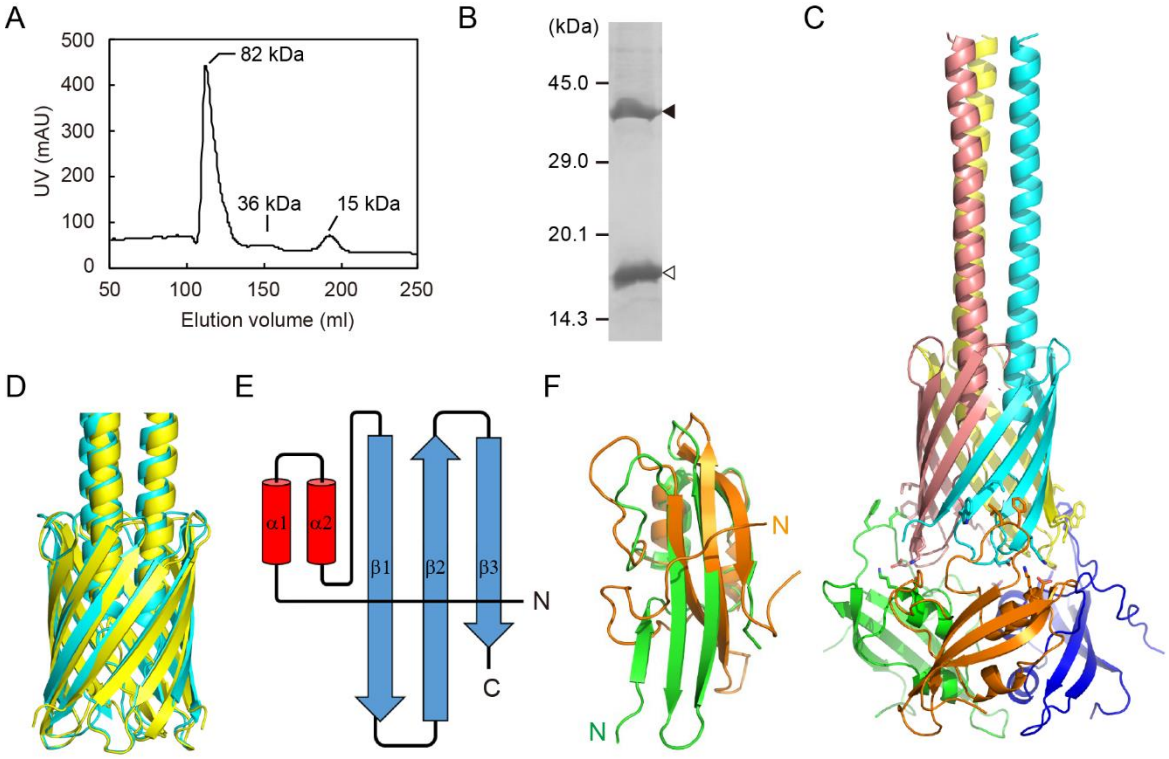

Figure 2. Crystal structure of the transmembrane domain of AtaA in complex with the N-terminal domain of TpgA. (A) Size-exclusion chromatography of the complex of AtaA-TM and TpgA-N. (B) The purified complex of AtaA-TM and TpgA-N was subjected to SDS–PAGE followed by CBB staining. The solid and open triangles indicate the AtaA-TM trimer and TpgA-N, respectively. (C) Overall structure of the AtaA-TM and TpgA-N complex. The AtaA-TM monomers are shown in cyan, pink and yellow, and the TpgA-N monomers are shown in orange, green and blue, respectively. (D) Comparison of the AtaA-TM (yellow) with the transmembrane domain of *H. influenzae* Hia (2GR7; cyan). (E) A topology diagram of TpgA-N. α-helices are shown as cylinders, and β-strands are shown as arrows. (F) Comparison of TpgA-N (orange) with *E. coli* BamE (5D0Q; green).

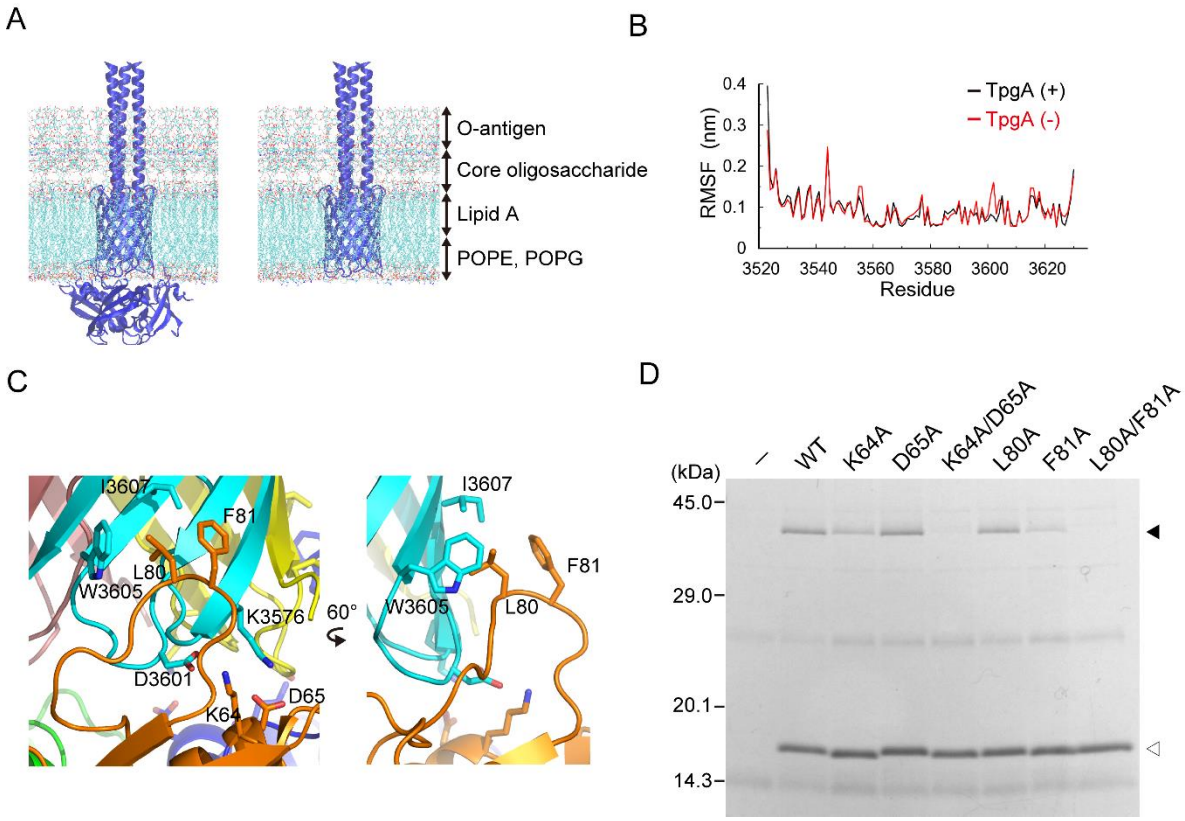

Figure 3. Interaction between the transmembrane domain of AtaA and the N-terminal domain of TpgA.

(A) A snapshot from the MD simulation of AtaA-TM and TpgA-N. Polypeptides of AtaA-TM and TpgA-N are shown as cartoon models in blue, and phospholipids and lipopolysaccharides (LPS) are shown in line representation. (B) The root mean square fluctuation (RMSF) of each residue of AtaA-TM calculated from 500-ns simulation. (C) Enlarged views showing hydrophobic and electrostatic interactions between AtaA-TM (cyan) and TpgA-N (orange). The interacting residues are shown in stick representation. (D) Pull-down assay of AtaA-TM and mutated TpgA-N. Cell lysate containing AtaA-TM was mixed with His-tagged TpgA-N-bound Ni-NTA beads or untreated beads as a control (-). The pulled-down proteins were subjected to SDS–PAGE and detected by CBB staining. The solid and open triangles indicate the AtaA-TM and point-mutated TpgA-N proteins, respectively.

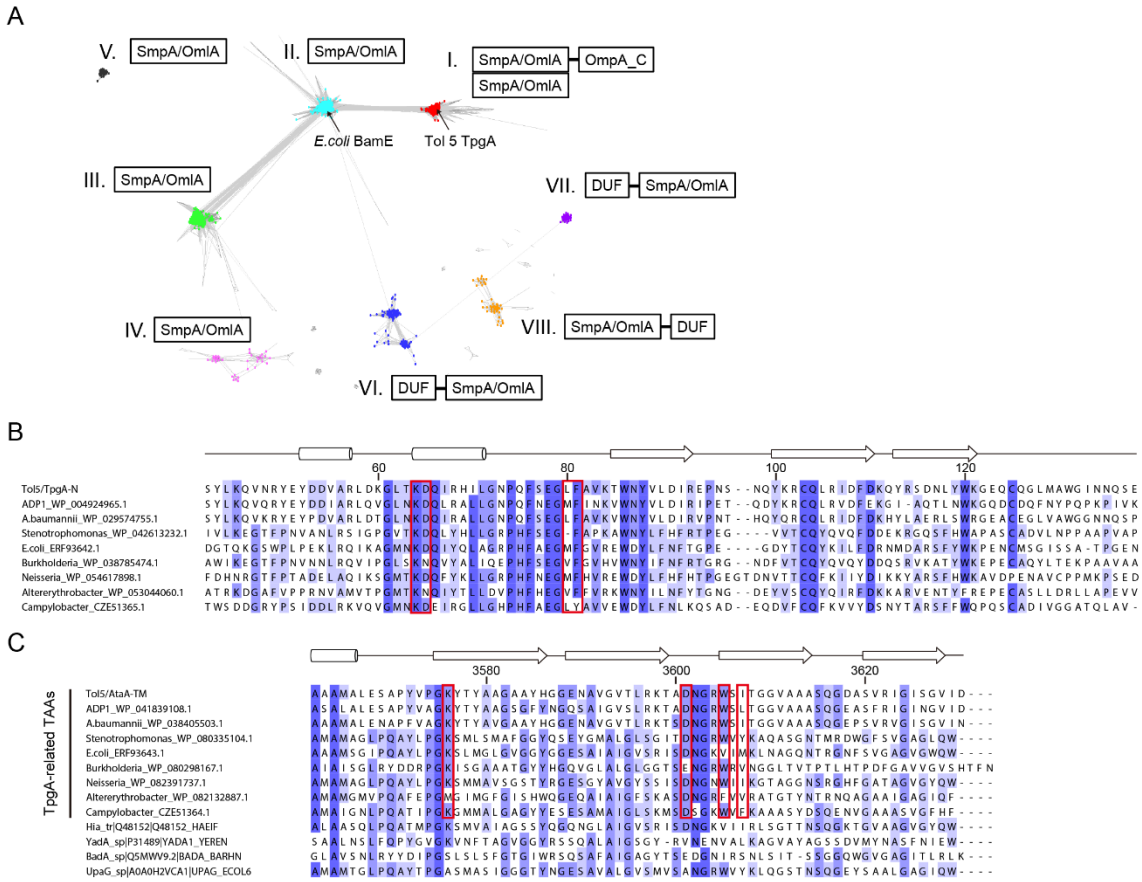

Figure 4. Bioinformatic analysis of the N-terminal domain of TpgA and the transmembrane domain of AtaA. (A) Cluster map of SmpA/OmlA family proteins. The map represents individual proteins and their sequence similarities as dots and gray lines, respectively. The positions of TpgA of Tol 5 and BamE of *E.coli* are indicated by arrows. (B) Amino acid sequence of the TpgA-N and TpgA-like proteins found in cluster I. Red boxes indicate residues that interact with AtaA. (C) Amino acid sequence of the C-terminal domain of AtaA; other TAAs found upstream of *tpgA*-like genes in the genome; and four representative TAAs (Hia, YadA, BadA, and UpaG) not related to TpgA. The red boxes indicate residues that interact with TpgA.

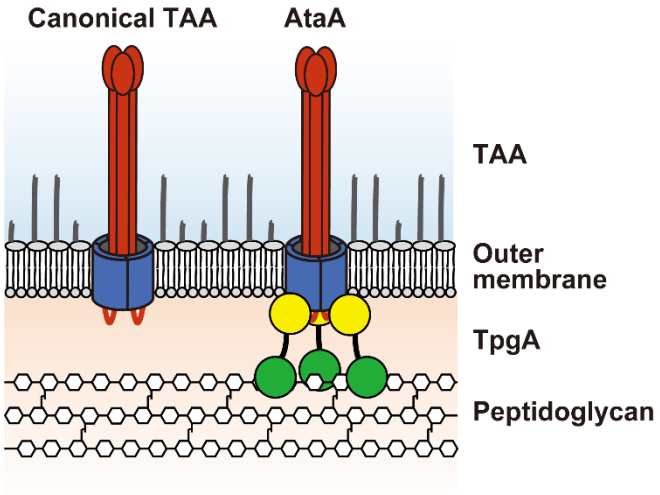

Figure 5. Schematic representation of a canonical TAA and the AtaA-TpgA-peptidoglycan complex. The passenger and transmembrane domains of TAAs are shown in red and blue, respectively. The N-terminal and C-terminal domains of TpgA are shown in yellow and green, respectively.